Chemical Physics Letters 683 (2017) 300–305

Contents lists available at ScienceDirect

Chemical Physics Letters

journal homepage: www.elsevier.com/locate/cplett

Research paper

Comparison of ultrafast electron and X-ray diffraction – A computational study

Minas Stefanou [a], Kenichiro Saita [a], Dmitrii V. Shalashilin [b], Adam Kirrander [a,*]

[a] EaStCHEM, School of Chemistry, University of Edinburgh, David Brewster Road, Edinburgh EH9 3FJ, United Kingdom
[b] School of Chemistry, University of Leeds, Leeds LS2 9JT, United Kingdom

ARTICLE INFO

Article history:
Received 21 December 2016
In final form 4 March 2017
Available online 7 March 2017

2010 MSC:
00-01
99-00

Keywords:
Quantum molecular dynamics
Ultrafast electron diffraction
Ultrafast X-ray scattering
Ethylene
Photochemistry

ABSTRACT

We compare ultrafast electron and X-ray diffraction using quantum molecular dynamics simulations in photoexcited ethylene. The simulations of ethylene are done using the *ab-initio* multiconfigurational Ehrenfest (AI-MCE) approach, with electronic structure calculations at the SA3-CASSCF(2,2)/cc-ppVDZ level. The diffraction signal is calculated using the independent atom model. We find that the electron diffraction is more sensitive to the nuclear wavepacket, and the dynamics of the hydrogen atoms in particular.

1. Introduction

Ultrafast laser spectroscopy has developed dramatically over the past two decades, and constitutes today a large family of techniques capable of probing fundamental transformations of matter in astonishing detail [1,2]. However, spectroscopy probes molecular rearrangements of geometry indirectly, in energy rather than in spatial coordinates, and inversion of the observed spectra often requires extensive high-level calculations. In contrast, diffraction probes molecular geometry directly. This key advantage was recognised by Ahmed Zewail, who even before his 1999 Nobel Prize was working on ultrafast electron diffraction (UED) [3] and continued to pursue it vigorously after the Prize [4,5], in the footsteps of and alongside other pioneers [6–8].

The bet on electron diffraction was clever, because it echoed a similar development in the early days of static gas-phase diffraction [9,10], where electrons came to supersede X-rays thanks to the larger scattering cross-section. However, interest in time-resolved X-ray diffraction remained [11], and new experiments suitable for time-resolved X-ray scattering in the condensed phase were developed using mechanical choppers at synchrotrons [12].

The emergence of X-ray Free-Electron Lasers (XFELs) put X-ray diffraction firmly back in the picture by offering a large increase in X-ray intensity and short pulse durations [13], making ultrafast X-ray diffraction possible both in gas [14–19] and condensed phases [20,21]. In parallel, the introduction of high-energy electron beams overcame the space-charge and velocity mismatch problems that previously hampered the time-resolution of UED [22,23].

This brings us to the current and rather promising situation, where we have two powerful ultrafast diffraction techniques, one based on electrons and one on X-rays, both capable of complementing ultrafast spectroscopy. This Letter, in recognition of Ahmed Zewail's contributions to ultrafast spectroscopy, femtochemistry, and UED, compares the electron and X-ray diffraction signals predicted for the ultrafast dynamics of photoexcited ethylene using state-of-the-art quantum molecular dynamics simulations, with the aim of exploring the complementarities of ultrafast diffraction by either electrons or X-rays.

2. Theory

The photodynamics of the excited ethylene molecule ($H_2C{=}CH_2$) is simulated using the AI-MCE quantum molecular dynamics method [24,25], which is derived from the coupled coherent states methodology [26–28]. The molecular wavefunction, $|\Psi(t)\rangle$, is

* Corresponding author.
E-mail address: Adam.Kirrander@ed.ac.uk (A. Kirrander).

http://dx.doi.org/10.1016/j.cplett.2017.03.007
0009-2614/

expanded in terms of Ehrenfest wavepackets with dynamically coupled expansion coefficients $D_k(t)$,

$$|\Psi(t)\rangle = \sum_{k=1}^{N} D_k(t)|\psi_k(t)\rangle, \tag{1}$$

where each individual wavepacket, $|\psi_k(t)\rangle$, consists of a nuclear wavepacket, $|\bar{\mathbf{z}}_k(t)\rangle$, distributed across multiple electronic states, $|\phi_k^i\rangle$, with amplitudes $a_k^i(t)$,

$$|\psi_k(t)\rangle = \left[\sum_{i=1}^{N_s} a_k^i(t)|\phi_k^i\rangle\right]|\bar{\mathbf{z}}_k(t)\rangle. \tag{2}$$

For larger molecules and complicated dynamics, converging the expansion in Eq. (1) is challenging but sampling methods have been developed to speed up convergence [29,30]. The electronic potential energies, gradients, and nonadiabatic couplings required for the simulations are calculated *on-the-fly* at the SA3-CASSCF level using the MOLPRO electronic structure package [31]. A small but balanced CAS(2,2) active space is used together with the Dunning's cc-ppVDZ basis [25]. The Ehrenfest trajectories are initiated in the Franck-Condon region using a Wigner distribution [32], with initial population completely localised on the first excited S_1 ($\pi\pi^*$) state, and are propagated for 150 fs with a total of 1000 Ehrenfest trajectories included, resulting in a converged calculation [25].

Next we calculate the time-dependent X-ray and electron diffraction signals for the photoexcited ethylene using the independent atom model (IAM) approximation for elastic scattering with the assumption of a negligible coherence length of the probe pulse relative the time-scale of the dynamics. This results in an incoherent convolution from different molecular geometries present in the wavepacket [33]. Thus, the differential scattering cross-section is a convolution of the instantaneous scattering signal $\mathcal{W}(\tau, q)$ [33],

$$dS(\mathbf{q}, t_p) = \alpha \int_0^\infty I_P(\tau - t_p)\, \mathcal{W}(\tau, \mathbf{q})\, d\tau, \tag{3}$$

where $I_P(\tau)$ is the intensity profile of the probe pulse, t_p is the delay time between pump and probe pulses, and the pre-factor α provides an overall scaling of the signal which is different for electrons and X-rays, and is left out in the present comparison. The momentum transfer vector $\mathbf{q}$ is the difference between the incident and scattered wave vectors, and has amplitude $|\mathbf{q}| = (4\pi/\lambda)\sin(\theta/2)$, with θ the deflection angle and λ the (de Broglie) wavelength. In electron diffraction the conventional symbol for the momentum transfer is $\mathbf{s}$ rather than $\mathbf{q}$, and we use the two symbols interchangeably.

Since the IAM does not distinguish between different electronic states, the signal depends only on molecular geometry,

$$\mathcal{W}(\tau, \mathbf{q}) = \langle \Psi(\tau; \bar{\mathbf{R}})|\, |f_{\mathrm{IAM}}(\mathbf{q}; \bar{\mathbf{R}})|^2\, |\Psi(\tau; \bar{\mathbf{R}})\rangle_{\bar{\mathbf{R}}}, \tag{4}$$

with the integration over the nuclear coordinates $\bar{\mathbf{R}}$, amounting to a convolution of the IAM scattering over the total nuclear wavefunction [33].

The explicit form of the IAM form factor $f_{\mathrm{IAM}}(\mathbf{q}; \bar{\mathbf{R}})$ is different for X-rays and electrons. In practice, the X-rays scatter only from the electron density, resulting in,

$$f_{\mathrm{IAM}}^{\mathrm{xray}}(\mathbf{q}; \bar{\mathbf{R}}) = \sum_{\alpha=1}^{N_{\mathrm{at}}} f_\alpha^0(q) e^{i\mathbf{R}_\alpha \mathbf{q}}, \tag{5}$$

where $f_\alpha^0(q)$ are the tabulated atomic form factors [34], N_{at} the number of atoms, and $\mathbf{R}_\alpha$ the position of atom α. In contrast, the electrons scatter from the total charge density. Assuming that the nuclei are point charges we obtain,

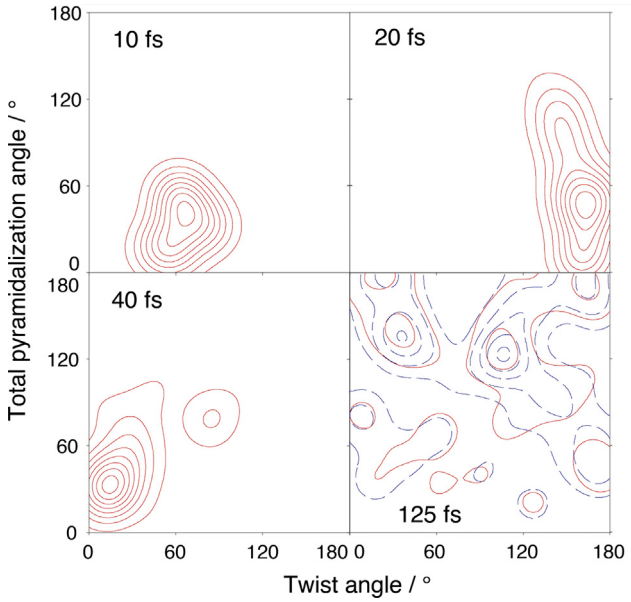

Fig. 1. Contour plot showing the probability distribution of the C—C twist angle and the degree of pyramidalisation of the carbon atoms at times $t = 10, 20, 40$, and 125 fs.

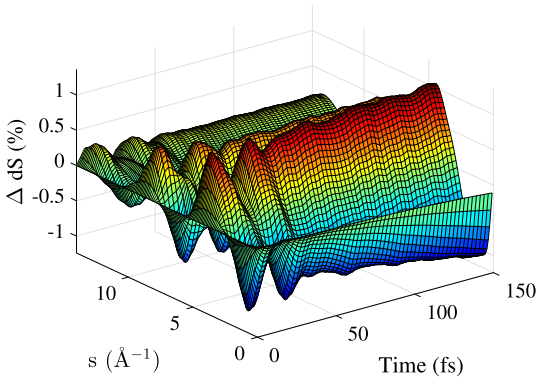

(a) 1000 trajectories

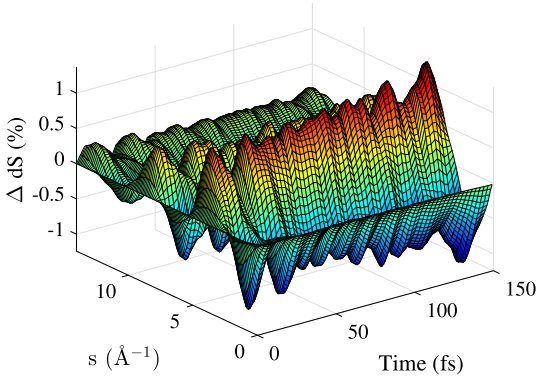

(b) 20 trajectories

Fig. 2. Elastic electron scattering difference signal, $\Delta dS^{\mathrm{elec}}(s, t)$, in percent, shown as a function of momentum transfer s and pump-probe delay-time t, calculated using Eq. (8) with rotational averaging for photoexcited ethylene. The upper figure shows the signal calculated for 1000 trajectories, while the lower shows the signal for a subset of 20 trajectories.

$$f_{\mathrm{IAM}}^{\mathrm{elec}}(\mathbf{s}; \bar{\mathbf{R}}) = \sum_{\alpha=1}^{N_{\mathrm{at}}} \frac{Z_i - f_\alpha^0(s)}{s^2} e^{i\mathbf{R}_\alpha \mathbf{s}}, \tag{6}$$

where Z_i is the atomic number of each nucleus. The scattering from the electron density is included via the same atomic form factors as in X-ray scattering, and is added coherently to the scattering from the nuclei. The expression for electron scattering is quite similar to Eq. (5), apart from an overall damping factor s^{-2}. The treatment of electron scattering could be improved by compensating for failures in the Born-approximation via atomic phase-factors η_α and relativistic corrections (an overview is provided in Section 4.3.3.3 of Ref. [34]).

In the following, we consider rotationally averaged scattering (mean intensity) along the lines of Debye's well-known derivation [35], which results in an intensity $\langle|f_{\mathrm{IAM}}(q)|^2\rangle_{\mathrm{rot}}$ that depends only on the amplitude of the momentum transfer and the distance between atoms, $R_{\alpha\beta} = |\mathbf{R}_\alpha - \mathbf{R}_\beta|$,

$$\langle|f_{\mathrm{IAM}}(q)|^2\rangle_{\mathrm{rot}} = \sum_{\alpha=1}^{N_{\mathrm{at}}}|f_\alpha^0(q)|^2 + \sum_{\beta\neq\alpha}^{N_{\mathrm{at}}} f_\alpha^0(q) f_\beta^0(q)\frac{\sin(qR_{\alpha\beta})}{qR_{\alpha\beta}}, \tag{7}$$

shown here for X-ray scattering, and with an analogous expression for electron scattering. The first sum on the right-hand side is the atomic scattering term, $I_{\mathrm{at}}(q)$, and the second is the molecular term, $I_{\mathrm{mol}}(q)$, which contains the interference that yields structural information.

3. Results

Ethylene photodynamics has been studied extensively, both experimentally [36] and theoretically [25,37], and our AI-MCE simulations are broadly in agreement with previous simulations which exclude the contribution of Rydberg states [25,37]. Following vertical excitation into the S_1 ($\pi\pi^*$) state, the ethylene molecule undergoes cis-trans isomerisation around the C=C bond, and decays via nonradiative decay through a twisted or pyramidalised conical intersection, or via H-atom migration to form ethylidene (CH_3CH) which then decays through a different conical intersection.

The population of S_1 remains fairly constant for the first 30 fs, at which point the molecule reaches a region where the gap between S_1 and S_0 is sufficiently small for efficient population transfer, and the population then decays exponentially with an approximate lifetime of $\approx$ 112 fs. As can be seen in Fig. 1, the wavepacket disperses rather quickly.

The diffraction signal is given in terms of the percentage difference signal, $\Delta dS(q,t)$, defined as,

$$\Delta dS(q,t) = \gamma_{\mathrm{excit}}\frac{dS(q,t) - dS_{\mathrm{off}}(q)}{dS_{\mathrm{off}}(q)}, \tag{8}$$

where γ_{excit} is the fraction of excited molecules, $dS(q,t)$ is the *laser-on* signal corresponding to the molecular wavefunction excited by the pump pulse, $dS_{\mathrm{off}}(q)$ is the *laser-off* background signal, and we drop the subscript on t_P. In the calculations a Gaussian-profile probe pulse with duration 25 fs is assumed, with the q/s-range up to 14 Å^{-1} and an excitation fraction of 9%.

The resulting diffraction signal, $\Delta dS^{\mathrm{elec}}(s,t)$, is shown in Fig. 2a. At short times the coherent oscillation in the C—C bond-length leaves a distinct signature, while at later times the signal becomes progressively more constant as increasing dispersion and delocalisation of the nuclear wavefunction averages out specific motions. The main three factors that influence the diffraction signal are the oscillations in the C—C distance, the pyramidalisation and twist around the C—C bond, and the dispersion of the molecular wavepacket.

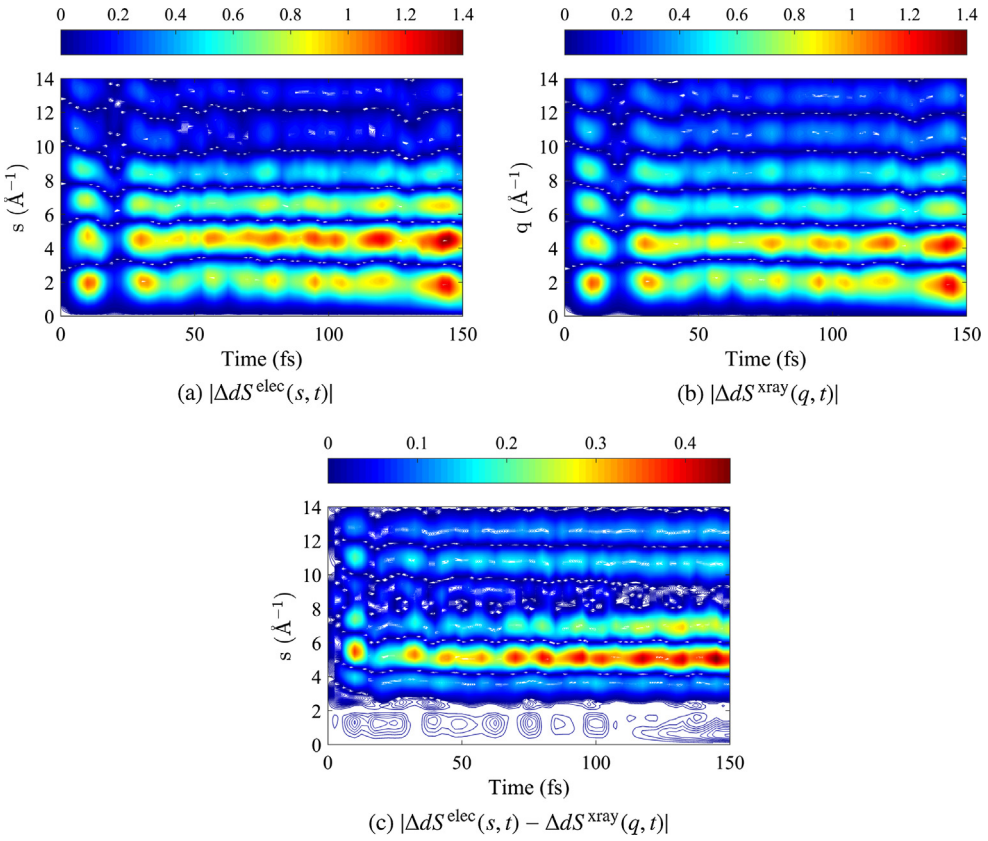

Fig. 3. Contour plots of the elastic scattering signal for photoexcited ethylene, plotted against the momentum transfer s (q for X-rays) and pump-probe delay-time t, for electron (Fig. 3a) and X-ray (Fig. 3b) scattering respectively. Fig. 3c shows the absolute difference between electrons and X-rays.

The sensitivity of the calculated scattering signal to the number of included Ehrenfest trajectories can be assessed from comparison of Fig. 2a, which shows the signal calculated for 1000 trajectories, and Fig. 2b, which is calculated using 20 trajectories. The smaller subset captures the main features of the scattering signal quite well, but underestimates the dispersion of the nuclear wavepacket at longer times, as can be seen from the comparatively sharp features present in the small set at long times, but absent from the large set. The reminder of the calculations in this Letter are done with the smaller subset in Fig. 2b. Overall, the electron diffraction signal calculated here agrees with the X-ray signal calculated previously [33].

To examine the differences between the X-ray and the electron diffraction, we calculate the absolute difference of the diffraction signals, $|\Delta dS^{\mathrm{elec}}(s,t) - \Delta dS^{\mathrm{xray}}(q,t)|$, with the results shown in Fig. 3c. The non-negligible difference between the two diffraction signals stems from the greater contrast (variation) in the electron diffraction signal, which ultimately can be traced to the additional contributions from the nuclei. The difference is very small in the small angle scattering, but increases at intermediate angles and remains fairly significant to 11 $\mathrm{Å}^{-1}$, corresponding to comparatively high resolution. The difference also appears to increase over time, an issue that we will address below.

We proceed to demonstrate that a large part of the difference between the electron and X-ray scattering signal stems from the greater sensitivity of electron scattering to nuclear motion. In ethylene, at longer times the most distinct motion is associated with the hydrogen atoms, while the carbon-carbon dynamics is strongly dispersed. Using "computational *alchemy*" we set all distances associated with the H-atoms to large values (>1000 Å), thus quenching the contribution of the H-atoms to the structural interference term (I_{mol}), while leaving their contribution to the atomic scattering (I_{at}) unaffected. We examine the effect of this modification, by plotting $\left|\Delta dS^{\mathrm{elec}}_{\mathrm{norm}}(s,t) - \Delta dS^{\mathrm{elec}}_{\mathrm{mod}}(s,t)\right|$ with the "modified" diffraction, $\Delta dS^{\mathrm{elec}}_{\mathrm{mod}}(s,t)$, corresponding to the ethylene signal with quenched H-atoms and the "normal" diffraction, $\Delta dS^{\mathrm{elec}}_{\mathrm{norm}}(s,t)$, corresponding to the regular diffraction obtained with normal distances.

The results are shown in Fig. 4. The main differences between the "modified" and the "normal" diffraction appear in the interval $2 < q < 8$ $\mathrm{Å}^{-1}$ for both electrons (Fig. 4a) and X-rays (Fig. 4b). It is clear from the two contour plots, both plotted using the same color axis, that the effect of the H-atoms on the diffraction pattern is far greater for electron diffraction. Looking at the electron diffraction in Fig. 4a there is also a comparative increase in the difference signal over time, which is largely absent in the X-ray diffraction in Fig. 4b. This leads to the conclusion that the increased difference between electron and X-ray diffraction observed at long times in Fig. 3c can be ascribed to diffraction from the small amplitude motion of the H-atoms, emphasising the sensitivity of electron diffraction to nuclear dynamics.

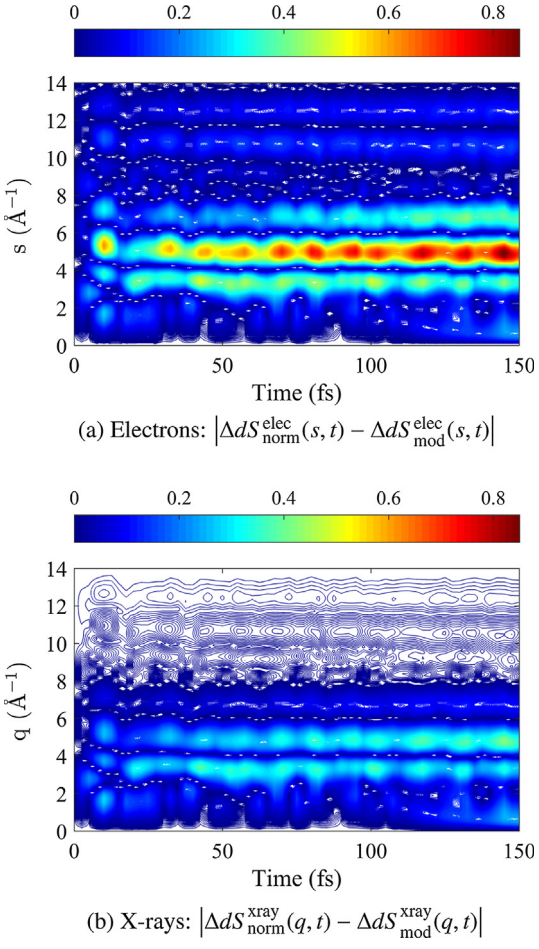

Fig. 4. Contour plots of "normal" vs "modified" ethylene diffraction plotted as a function of the momentum transfer s (q for X-rays) and the pump-probe delay-time t. In the modified case, the contribution to the structural component of the diffraction from the H-atoms has been quenched. Fig. 4a shows the difference between normal and modified diffraction for electron diffraction, while Fig. 4b shows the same difference for X-rays.

4. Conclusions

Our quantum molecular dynamics simulations of photoexcited ethylene and the calculated diffraction signals for X-rays and electrons show that the signals from ultrafast electron and X-ray diffraction are qualitatively similar. Although both signals carry signatures of the dominant carbon-carbon dynamics at short times, the electron diffraction is more sensitive to the dynamics of the hydrogen atoms at long times when the carbon-carbon portion of the wavepacket is strongly dispersed. This is not surprising given that the electron beam probes the nuclei directly, while in the X-ray scattering the nuclear motion is probed indirectly via the comparatively diffuse electron densities of the atoms.

One of the greatest advantages of X-rays may lie in their versatility, since they are not just capable of ultrafast X-ray diffraction but also of e.g. X-ray spectroscopy [38], inelastic Raman scattering [39], and Coulomb explosion imaging [40]. In general, a promising future direction for both electron and X-ray diffraction is the combination of energy-resolved and spatially-resolved measurements, with a recent example of this a combined photoelectron spectroscopy and ultrafast X-ray diffraction study of the ring-opening reaction in 1,3-cyclohexadiene [41].

Finally, it is worth pointing out that the independent atom model (IAM) is a simplified model of the elastic scattering. Accounting for the actual electron density of the target is known to result in differences in the elastic scattering, something which may potentially be exploited to distinguish different electronic states [42,43]. Polarisation of the electron density, for instance around hydrogen atoms, is known to require corrections beyond the IAM model [44,45,42], and the additional scattering from the nuclei afforded by electrons is useful in those situations. It would be interesting to see UED data for the ultrafast dynamics of H_2 or D_2 in the gas-phase [46], or perhaps for tunneling in photoexcited dimer-molecules [47]. Looking further into the future, one may envision the detection of electronic structure using X-ray or electron scattering [48,49,42,50].

Acknowledgements

AK and KS acknowledge funding from the Leverhulme Trust (RPG-2013-365) and AK acknowledges additional funding from the European Union (FP7-PEOPLE-2013-CIG-NEWLIGHT). MS acknowledges a PhD studentship from the University of Edinburgh (Chemistry). KS and DS were supported by the EPSRC Grants Number EP/I014500/1 and EP/J001481/1. DS would also like to acknowledge current support from EPSRC Grant No. EP/N007549/1.

References

[1] A. Kirrander, R.S. Minns, Highlights from faraday discussion 194: ultrafast imaging of photochemical dynamics, Chem. Commun. 52 (2016) 13631–13636, http://dx.doi.org/10.1039/C6CC90504H.
[2] R.J.D. Miller, Ultrafast imaging of photochemical dynamics: roadmap to a new conceptual basis for chemistry, Faraday Discuss. 194 (2016) 777–828, http://dx.doi.org/10.1039/C6FD00241B.
[3] J. Williamson, M. Dantus, S. Kim, A. Zewail, Ultrafast diffraction and molecular structure, Chem. Phys. Lett. 196 (6) (1992) 529–534, http://dx.doi.org/10.1016/0009-2614(92)85988-M.
[4] H. Ihee, V.A. Lobastov, U.M. Gomez, B.M. Goodson, R. Srinivasan, C.-Y. Ruan, A. H. Zewail, Direct imaging of transient molecular structures with ultrafast diffraction, Science 291 (5503) (2001) 458–462, http://dx.doi.org/10.1126/science.291.5503.458.
[5] A.H. Zewail, Four-dimensional electron microscopy, Science 328 (5975) (2010) 187–193, http://dx.doi.org/10.1126/science.1166135.
[6] A.A. Ischenko, V.V. Golubkov, V.P. Spiridonov, A.V. Zgurskii, A.S. Akhmanov, M. G. Vabischevich, V.N. Bagratashvili, A stroboscopical gas-electron diffraction method for the investigation of short-lived molecular species, Appl. Phys. B 32 (3) (1983) 161–163, http://dx.doi.org/10.1007/BF00688823.
[7] R.C. Dudek, P.M. Weber, Ultrafast diffraction imaging of the electrocyclic ring-opening reaction of 1,3-cyclohexadiene, J. Phys. Chem. A 105 (17) (2001) 4167–4171, http://dx.doi.org/10.1021/jp010122t.
[8] B.J. Siwick, J.R. Dwyer, R.E. Jordan, R.J.D. Miller, An atomic-level view of melting using femtosecond electron diffraction, Science 302 (5649) (2003) 1382–1385, http://dx.doi.org/10.1126/science.1090052.
[9] P. Debye, L. Bewilogua, F. Ehrhardt, Zerstreuung von Röntgenstrahlen an einzelnen Molekülen (vorläufige Mitteilung), Phys. Zeits. 30 (1929) 84.
[10] R. Wierl, Elektronenbeugung und Molekülbau. II, Ann. Phys. 405 (1932) 453–482, http://dx.doi.org/10.1002/andp.19324050405.
[11] J.P. Bergsma, M.H. Coladonato, P.M. Edelsten, J.D. Kahn, K.R. Wilson, D.R. Fredkin, Transient X-ray scattering calculated from molecular dynamics, J. Chem. Phys. 84 (1986) 6151–6160, http://dx.doi.org/10.1063/1.450756.
[12] R. Neutze, R. Wouts, S. Techert, J. Davidsson, M. Kocsis, A. Kirrander, F. Schotte, M. Wulff, Visualizing photochemical dynamics in solution through picosecond X-ray scattering, Phys. Rev. Lett. 87 (19) (2001) 195508, http://dx.doi.org/10.1103/PhysRevLett.87.195508.
[13] C. Bostedt, J.D. Bozek, P.H. Bucksbaum, R.N. Coffee, J.B. Hastings, Z. Huang, R.W. Lee, S. Schorb, J.N. Corlett, P. Denes, P. Emma, R.W. Falcone, R.W. Schoenlein, G. Doumy, E.P. Kanter, B. Kraessig, S. Southworth, L. Young, L. Fang, M. Hoener, N. Berrah, C. Roedig, L.F. DiMauro, Ultra-fast and ultra-intense X-ray sciences: first results from the Linac Coherent Light Source free-electron laser, J. Phys. B: At. Mol. Opt. Phys. 46 (2013) 164003, http://dx.doi.org/10.1088/0953-4075/46/16/164003.
[14] J. Küpper, S. Stern, L. Holmegaard, F. Filsinger, A. Rouzée, A. Rudenko, P. Johnsson, A.V. Martin, M. Adolph, A. Aquila, S. Bajt, A. Barty, C. Bostedt, J. Bozek, C. Caleman, R. Coffee, N. Coppola, T. Delmas, S. Epp, B. Erk, L. Foucar, T. Gorkhover, L. Gumprecht, A. Hartmann, R. Hartmann, G. Hauser, P. Holl, A. Hömke, N. Kimmel, F. Krasniqi, K.-U. Kühnel, J. Maurer, M. Messerschmidt, R. Moshammer, C. Reich, B. Rudek, R. Santra, I. Schlichting, C. Schmidt, S. Schorb, J. Schulz, H. Soltau, J.C.H. Spence, D. Starodub, L. Strüder, J. Thøgersen, M.J.J. Vrakking, G. Weidenspointner, T.A. White, C. Wunderer, G. Meijer, J. Ullrich, H. Stapelfeldt, D. Rolles, H.N. Chapman, X-ray diffraction from isolated and strongly aligned gas-phase molecules with a free-electron laser, Phys. Rev. Lett. 112 (8) (2014) 083002, http://dx.doi.org/10.1103/PhysRevLett.112.083002.
[15] M.P. Minitti, J.M. Budarz, A. Kirrander, J. Robinson, T.J. Lane, D. Ratner, K. Saita, T. Northey, B. Stankus, V. Cofer-Shabica, J. Hastings, P.M. Weber, Toward structural femtosecond chemical dynamics: imaging chemistry in space and time, Faraday Discuss. 171 (2014) 81–91, http://dx.doi.org/10.1039/C4FD00030G.
[16] M.P. Minitti, J.M. Budarz, A. Kirrander, J.S. Robinson, D. Ratner, T.J. Lane, D. Zhu, J.M. Glownia, M. Kozina, H.T. Lemke, M. Sikorski, Y. Feng, S. Nelson, K. Saita, B. Stankus, T. Northey, J.B. Hastings, P.M. Weber, Imaging molecular motion: femtosecond X-ray scattering of an electrocyclic chemical reaction, Phys. Rev. Lett. 114 (25) (2015) 255501, http://dx.doi.org/10.1103/PhysRevLett.114.255501.
[17] J.M. Budarz, M.P. Minitti, D.V. Cofer-Shabica, B. Stankus, A. Kirrander, J.B. Hastings, P.M. Weber, Observation of femtosecond molecular dynamics via pumpprobe gas phase X-ray scattering, J. Phys. B: At. Mol. Opt. Phys. 49 (3) (2016) 034001, http://dx.doi.org/10.1088/0953-4075/49/3/034001.
[18] B. Stankus, J.M. Budarz, A. Kirrander, D. Rogers, J. Robinson, T.J. Lane, D. Ratner, J. Hastings, M.P. Minitti, P.M. Weber, Femtosecond photodissociation dynamics of 1,4-diiodobenzene by gas-phase X-ray scattering and photoelectron spectroscopy, Faraday Discuss. 194 (2016) 525–536, http://dx.doi.org/10.1039/C6FD00135A.
[19] J.M. Glownia, A. Natan, J.P. Cryan, R. Hartsock, M. Kozina, M.P. Minitti, S. Nelson, J. Robinson, T. Sato, T. van Driel, G. Welch, C. Weninger, D. Zhu, P.H. Bucksbaum, Self-referenced coherent diffraction X-ray movie of Ångström- and femtosecond-scale atomic motion, Phys. Rev. Lett. 117 (15) (2016) 153003, http://dx.doi.org/10.1103/PhysRevLett.117.153003.
[20] M. Lebantino, G. Schiro, H.T. Lemke, G. Cottone, J.M. Glownia, D. Zhu, M. Chollet, H. Ihee, A. Cupane, M. Cammarata, Ultrafast myoglobin structural dynamics observed with an X-ray free-electron laser, Nature Comm. 6 (2015), http://dx.doi.org/10.1038/ncomms7772 Article number: 6772.
[21] K.H. Kim, J.G. Kim, S. Nozawa, T. Sato, K.Y. Oang, T.W. Kim, H. Ki, J. Jo, S. Park, C. Song, T. Sato, K. Ogawa, T. Togashi, K. Tono, M. Yabashi, T. Ishikawa, J. Kim, R. Ryoo, J. Kim, H. Ihee, S.i. Adachi, Direct observation of bond formation in solution with femtosecond X-ray scattering, Nature 518 (7539) (2015) 385–389, http://dx.doi.org/10.1038/nature14163.
[22] J. Yang, M. Guehr, T. Vecchione, M.S. Robinson, R. Li, N. Hartmann, X. Shen, R. Coffee, J. Corbett, A. Fry, K. Gaffney, T. Gorkhover, C. Hast, K. Jobe, I. Makasyuk, A. Reid, J. Robinson, S. Vetter, F. Wang, S. Weathersby, C. Yoneda, M. Centurion, X. Wang, Diffractive imaging of a rotational wavepacket in nitrogen molecules with femtosecond megaelectronvolt electron pulses, Nat. Comm. 7 (2016) 11232, http://dx.doi.org/10.1038/ncomms11232.
[23] J. Yang, M. Guehr, X. Shen, R. Li, T. Vecchione, R. Coffee, J. Corbett, N.H.A. Fry, C. Hast, K. Hegazy, K. Jobe, I. Makasyuk, J. Robinson, M.S. Robinson, S. Vetter, S. Weathersby, C. Yoneda, X. Wang, M. Centurion, Diffractive Imaging of Coherent Nuclear Motion in Isolated Molecules, Phys. Rev. Lett. 117 (15) (2016) 153002, http://dx.doi.org/10.1103/PhysRevLett.117.153002.
[24] D.V. Shalashilin, Nonadiabatic dynamics with the help of multiconfigurational ehrenfest method: improved theory and fully quantum 24d simulation of pyrazine, J. Chem. Phys. 132 (24) (2010) 244111, http://dx.doi.org/10.1063/1.3442747.
[25] K. Saita, D.V. Shalashilin, On-the-fly ab initio molecular dynamics with multiconfigurational Ehrenfest method, J. Chem. Phys. 137 (2012) 22A506, http://dx.doi.org/10.1063/1.4734313.
[26] D.V. Shalashilin, M.S. Child, The phase space CCS approach to quantum and semiclassical molecular dynamics for high-dimensional systems, Chem. Phys. 304 (1–2) (2004) 103–120, http://dx.doi.org/10.1016/j.chemphys.2004.06.013.
[27] D.V. Shalashilin, M.S. Child, A. Kirrander, Mechanisms of double ionization in strong laser field from simulation with Coupled Coherent States, Chem. Phys. 347 (1–3) (2008) 257–262, http://dx.doi.org/10.1016/j.chemphys.2007.11.006.
[28] A. Kirrander, D.V. Shalashilin, Quantum dynamics with fermion coupled coherent states, Phys. Rev. A 84 (3) (2011) 033406, http://dx.doi.org/10.1103/PhysRevA.84.033406.
[29] D.V. Makhov, W.J. Glover, T.J. Martinez, D.V. Shalashilin, Ab initio multiple cloning algorithm for quantum nonadiabatic molecular dynamics, J. Chem. Phys. 141 (5) (2014) 054110, http://dx.doi.org/10.1063/1.4891530.
[30] D.V. Makhov, K. Saita, T.J. Martinez, D.V. Shalashilin, Ab initio multiple cloning simulations of pyrrole photodissociation: Tker spectra and velocity map imaging, Phys. Chem. Chem. Phys. 17 (2015) 3316–3325, http://dx.doi.org/10.1039/C4CP04571H.
[31] H.-J. Werner, P.J. Knowles, G. Knizia, F.R. Manby, M. Schütz, et al., Molpro, version 2012.1, A Package of Ab Initio Programs. https://www.molpro.net/info/2015.1/doc/molpro.bib.
[32] R.C. Brown, E.J. Heller, Classical trajectory approach to photodissociation: the Wigner method, J. Chem. Phys. 75 (1) (1981) 186–188, http://dx.doi.org/10.1063/1.441822.
[33] A. Kirrander, K. Saita, D.V. Shalashilin, Ultrafast X-ray scattering from molecules, J. Chem. Theory Comput. 12 (2016) 957–967, http://dx.doi.org/10.1021/acs.jctc.5b01042.
[34] International Tables for Crystallography Volume C: Mathematical, physical and chemical tables, 2006th ed., no. ISBN 978-1-4020-1900-5, Wiley, 2006.
[35] P. Debye, Zerstreuung von Röntgenstrahlen, Ann. Phys. 351 (6) (1915) 809–823, http://dx.doi.org/10.1002/andp.19153510606.
[36] T. Kobayashi, T. Horio, T. Suzuki, Ultrafast deactivation of the $\pi\pi^*$(V) state of ethylene studied using sub-20 fs time-resolved photoelectron imaging, J. Phys. Chem. A 119 (36) (2015) 9518–9523, http://dx.doi.org/10.1021/acs.jpca.5b06094.
[37] T. Mori, W.J. Glover, M.S. Schuurman, T.J. Martinez, Role of rydberg states in the photochemical dynamics of ethylene, J. Phys. Chem. A 116 (11) (2012) 2808–2818, http://dx.doi.org/10.1021/jp2097185.
[38] M. Beye, H. Öberg, H. Xin, G.L. Dakovski, M. DellAngela, A. Föhlisch, J. Gladh, M. Hantschmann, F. Hieke, S. Kaya, D. Kühn, J. LaRue, G. Mercurio, M.P. Minitti, A. Mitra, S.P. Moeller, M.L. Ng, A. Nilsson, D. Nordlund, J. Norskov, H. Öström, H. Ogasawara, M. Persson, W.F. Schlotter, J.A. Sellberg, M. Wolf, F. Abild-Pedersen, L.G.M. Pettersson, W. Wurth, Chemical bond activation observed with an X-ray laser, J. Phys. Chem. Lett. 7 (18) (2016) 3647–3651, http://dx.doi.org/10.1021/acs.jpclett.6b01543.
[39] M. Kowalewski, K. Bennett, K.E. Dorfman, S. Mukamel, Catching conical intersections in the act: monitoring transient electronic coherences by attosecond stimulated X-ray raman signals, Phys. Rev. Lett. 115 (19) (2015) 193003, http://dx.doi.org/10.1103/PhysRevLett.115.193003.

[40] V.S. Petrović, M. Siano, J.L. White, N. Berrah, C. Bostedt, J.D. Bozek, D. Broege, M. Chalfin, R.N. Coffee, J. Cryan, L. Fang, J.P. Farrell, L.J. Frasinski, J.M. Glownia, M. Gühr, M. Hoener, D.M.P. Holland, J. Kim, J.P. Marangos, T. Martinez, B.K. McFarland, R.S. Minns, S. Miyabe, S. Schorb, R.J. Sension, L.S. Spector, R. Squibb, H. Tao, J.G. Underwood, P.H. Bucksbaum, Transient X-ray fragmentation: probing a prototypical photoinduced ring opening, Phys. Rev. Lett. 108 (25) (2012) 253006, http://dx.doi.org/10.1103/PhysRevLett.108.253006.

[41] C.C. Pemberton, Y. Zhang, K. Saita, A. Kirrander, P.M. Weber, From the (1B) spectroscopic state to the photochemical product of the ultrafast ring-opening of 1,3-cyclohexadiene: a spectral observation of the complete reaction path, J. Phys. Chem. A 119 (33) (2015) 8832–8845, http://dx.doi.org/10.1021/acs.jpca.5b05672.

[42] T. Northey, N. Zotev, A. Kirrander, Ab initio calculation of molecular diffraction, J. Chem. Theory Comput. 10 (11) (2014) 4911–4920, http://dx.doi.org/10.1021/ct500096r.

[43] A. Kirrander, X-ray diffraction assisted spectroscopy of Rydberg states, J. Chem. Phys. 137 (15) (2012) 154310, http://dx.doi.org/10.1063/1.4757913.

[44] R.F. Stewart, J. Bentley, B. Goodman, Generalized X-ray scattering factors in diatomic molecules, J. Chem. Phys. 63 (9) (1975) 3786–3793, http://dx.doi.org/10.1063/1.431871.

[45] T. Northey, A.M. Carrascosa, S. Schäfer, A. Kirrander, Elastic X-ray scattering from state-selected molecules, J. Chem. Phys. 145 (15) (2016) 154304, http://dx.doi.org/10.1063/1.4962256.

[46] A.R. Bainbridge, J. Harrington, A. Kirrander, C. Cacho, E. Springate, W.A. Bryan, R.S. Minns, VUV excitation of a vibrational wavepacket in D_2 measured through strong-field dissociative ionization, New J. Phys. 17 (2015) 103013, http://dx.doi.org/10.1088/1367-2630/17/10/103013.

[47] D.A. Horke, H.M. Watts, A.D. Smith, E. Jager, E. Springate, O. Alexander, C. Cacho, R.T. Chapman, R.S. Minns, Hydrogen bonds in excited state proton transfer, Phys. Rev. Lett. 117 (16) (2016) 163002, http://dx.doi.org/10.1103/PhysRevLett.117.163002.

[48] G. Dixit, O. Vendrell, R. Santra, Imaging electronic quantum motion with light, Proc. Natl. Acad. Sci. 109 (29) (2012) 11636–11640, http://dx.doi.org/10.1073/pnas.1202226109.

[49] H.-C. Shao, A.F. Starace, Imaging coherent electronic motion in atoms by ultrafast electron diffraction, Phys. Rev. A 88 (6) (2013) 062711, http://dx.doi.org/10.1103/PhysRevA.88.062711.

[50] H.J. Suominen, A. Kirrander, How to observe coherent electron dynamics directly, Phys. Rev. Lett. 112 (4) (2014) 043002, http://dx.doi.org/10.1103/PhysRevLett.112.043002.